Local structure of $Sr_2CuO_{3.3}$, a 95 K cuprate superconductor without CuO_2 planes

Steven D. Conradson[a,b], Theodore H. Geballe[c,d,e,1], Changqing Jin[f,g,h], Lipeng Cao[f], Gianguido Baldinozzi[i], Jack M. Jiang[c,e], Matthew J. Latimer[j], and Oliver Mueller[i]

[a]Department of Complex Matter, Jozef Stefan Institute, 1000 Ljubljana, Slovenia; [b]Department of Chemistry, Washington State University, Pullman, WA 99164; [c]Department of Applied Physics, Stanford University, Stanford, CA 94305; [d]Geballe Laboratory for Advanced Materials, Stanford University, Stanford, CA 94305; [e]Stanford Institute for Materials and Energy Science, SLAC National Accelerator Laboratory, Menlo Park, CA 94025; [f]Institute of Physics, Chinese Academy of Sciences, Beijing 100190, China; [g]School of Physics, University of Chinese Academy of Sciences, Chinese Academy of Sciences, Beijing 100190, China; [h]Materials Research Laboratory at Songshan Lake, Dongguan 523808, China; [i]Laboratoire Structures, Propriétés, et Modélisation des Solides, CNRS CentraleSupélec Université Paris-Saclay, F-91192 Gif-sur-Yvette Cedex, France; and [j]Stanford Synchrotron Radiation Lightsource, SLAC National Accelerator Laboratory, Menlo Park, CA 94025

Contributed by Theodore H. Geballe, December 19, 2019 (sent for review October 29, 2019; reviewed by Ivan Bozovic and Douglas J. J. Scalapino)

The local structure of the highly "overdoped" 95 K superconductor $Sr_2CuO_{3.3}$ determined by Cu K X-ray absorption fine structure (XAFS) at 62 K in magnetically oriented samples shows that 1) the magnetization is perpendicular to the *c* axis; 2) at these levels of precision the Cu sublattice is tetragonal in agreement with the crystal structure; the O sublattice has 3) continuous -Cu-O- chains that orient perpendicular to an applied magnetic field; 4) approximately half-filled -Cu-O- chains that orient parallel to this field; 5) a substantial number of apical O vacancies; 6) O ions at some apical positions with expanded Cu-O distances; and 7) interstitial positions that imply highly displaced Sr ions. These results contradict the universally accepted features of cuprates that require intact CuO_2 planes, magnetization along the *c* axis, and a termination of the superconductivity when the excess charge on the CuO_2 Cu ions exceeds 0.27. These radical differences in charge and structure demonstrate that this compound constitutes a separate class of Cu-O–based superconductors in which the superconductivity originates in a different, more complicated structural unit than CuO_2 planes while retaining exceptionally high transition temperatures.

overdoped cuprate | CuO_2 plane | high-temperature superconductivity | X-ray absorption fine structure spectroscopy

Although 135 K has remained the highest transition temperature in cuprates since 6 y after their initial discovery (1, 2), given that an accurate theory remains lacking, still higher transition temperatures cannot be ruled out. Here we report X-ray absorption fine structure (XAFS) experiments on $Sr_2CuO_{3.3}$ (SCO) prepared by high-pressure oxygen (HPO) methods that show that this compound lacks the CuO_2 planes found in all other cuprates while retaining a T_c of 95 K. The HPO cuprates (3–5) give a second, T_c vs. Cu-charge phase diagram whose superconducting region differs radically from the "dome" (6) common to the "conventional" materials that are doped by reaction with O_2. Instead of the superconductivity terminating with the formation of a Fermi liquid when the excess charge on the Cu atoms in the CuO_2 planes reaches ∼0.27 per Cu, T_c plateaus or even continues to increase, opening a new region of superconductivity on the high Cu-charge side of the phase diagram. In addition, these HPO cuprates are tetragonal, their heat capacities demonstrate coexisting Fermi liquid and superconducting electrons (7, 8), and they do not adhere to the empirical correlation between T_c and the Cu-apical O (Oap) (9–11) or apical cation (12) distance. $Ba_2CuO_{3.2}$ (8, 13, 14), a structural analog of SCO, exhibits an oblate Cu geometry with its Cu-Oap distance of less than 1.9 Å, presumably inverting the ordering of the $d_{x^2-y^2}$ and d_{z^2} states (8). SCO and related compounds were first prepared shortly after the initial discovery of cuprates (15). Jin and coworkers subsequently found multiple phases (16–18), but recent improvements in the synthesis now produce single-phase SCO with T_c = 95 K (*SI Appendix*, Fig. S1) (17, 18)

Between $La_2CuO_{4+\delta}$ and $Sr_2CuO_{3+\delta}$ (SCO) the structure changes radically. $La_2CuO_{4+\delta}$ exhibits the common cuprate geometry (19) with fully ordered CuO_2 planes with 3.78-Å Cu-Cu distances with O midway between, fully occupied Cu-Oap sites at 2.41 Å, and Cu-La at 3.24 Å. The structure of the other parent, Sr_2CuO_3 (20), is notable for its highly orthorhombic symmetry with -Cu-O- chains with a 3.91-Å Cu-Cu distance in the *a* direction and 3.48-Å Cu-Cu distances in the *b* direction that lacks bridging O. The disparate nature of the connections between the Cu sites along the crystallographic axes results in Sr_2CuO_3 being a "nearly ideal . . . [one-dimensional] . . . Heisenberg antiferromagnet" (21). The Oap sites are all occupied with the same 1.95 Cu-Oap distances as in the chains. This gives *c*-oriented $SrCuO_2$ planes with 3.22-Å Cu-Sr distances. Increasing the O stoichiometry by only ∼10% in HPO SCO results in its transformation to a tetragonal space group with a Cu-Cu distance of 3.8 Å that is typical of cuprates. However, its bulk stoichiometry with a fractional number of O atoms differs from the formula of its unit cell that is constrained to integers, and the absence of superlattice peaks demonstrates that these excess O atoms are distributed aperiodically (or dynamically). This disorder within the constraints of the tetragonal symmetry that presumably does not apply to the O sites causes ambiguities in the

Significance

CuO_2 planes are a universal component of cuprate superconductors. $Sr_2CuO_{3+\delta}$ that has a T_c of 95 K despite its overdoping has been reported to have vacancies in these planes. Extended X-ray absorption fine structure measurements not only provide definitive proof but furthermore show that in magnetically oriented samples not only are there also apical O vacancies but that the -Cu-O- chains normal to the orienting field are complete while the O sites of the chains parallel with this field are only half filled. These unique characteristics of a material with such a high transition temperature demonstrate that there are still substantial gaps in our knowledge of exotic superconductivity, including such fundamental aspects as the types of structures that support it.

Author contributions: S.D.C., T.H.G., and C.J. designed research; S.D.C., C.J., and J.M.J. performed research; C.J., L.C., G.B., M.J.L., and O.M. contributed new reagents/analytic tools; S.D.C. and G.B. analyzed data; and S.D.C. wrote the paper.

Reviewers: I.B., Brookhaven National Laboratory; and D.J.J.S., University of California, Santa Barbara.

The authors declare no competing interest.

[1]To whom correspondence may be addressed. Email: geballe@stanford.edu.

This article contains supporting information online at https://www.pnas.org/lookup/suppl/doi:10.1073/pnas.1918890117/-/DCSupplemental.

First published February 14, 2020.

crystallographic determination of its structure that include the possibility of vacancies in the CuO_2 planes (22, 23).

XAFS is arguably the most incisive experimental method for probing these behaviors in mixed valence, transition metal, correlated materials. It complements the crystallographic analysis of SCO because 1) it does not depend on long-range order or translational symmetry and therefore reveals aperiodic local lattice distortions; 2) its element selectivity separates and isolates many of the atom pairs to give a better basis for detailed analysis than X-ray or neutron pair distribution function analysis; and 3) its intrinsic time and energy scale that correspond to collective dynamical phenomena in correlated materials make it sensitive to the dynamical and instantaneous aspects of the structure, $S(q, \omega)$ or $S(q, t = 0)$ (24–28). The differences between the extended XAFS (EXAFS) (29, 30) and complementary diffraction and neutron scattering measurements (24, 31) were therefore key in originally identifying and characterizing the Cu-Oap double-well potential (32), its assignment to a tunneling polaron (25, 27, 33), and its coupling to the superconductivity in other cuprates (28, 34, 35). Tunneling polarons differ from the common small polarons that exhibit thermally activated hopping between neighboring sites in a crystal, exchanging the normal crystal structure adopted by the atoms at the second site with the distorted polaron structure and excess charge that had been at the first. A tunneling polaron is the oscillatory interchange between two distinct arrangements of a given set of atoms that contain the excess charge, with the two structures denoted by the charges and positions/local geometries of the constituent atoms. The tunneling polaron remains in the same location within a crystal, where it could be pinned because of stationary defects or special aspects of the atoms of its location. In addition, in contrast to the original, elementary, three-atom model of a Cu atom bracketed by two Oap, it may involve a large number of atoms and the two structures will be nondegenerate (36, 37).

A procedure that was key in these studies was the enhancement of the sensitivity of EXAFS to the different components of the structure (38) by orienting the samples in a magnetic field to align them along a unique crystallographic axis. The spectra therefore measure the projections of the neighbor atoms on the axis parallel to the orienting magnetic field and the plane perpendicular to it, rendering the problem one of cylindrical symmetry. The EXAFS will therefore help elucidate the characteristics of a crystallographically modulated structure (18), the widths of the distributions and whether they are continuous or consist of discrete, separated distances. The diffraction peaks of these samples were measured with the incident and diffracted X-rays in the plane normal to the axis along which the XAFS was measured (*SI Appendix*, Fig. S2). The (001) reflections of a $YBa_2Cu_3O_7$ and the two SCO samples were analyzed by the method of March and Dollase (39). The corresponding angular probability functions of the *c* crystallographic axis (Fig. 1) show that the E||H sample and E⊥H samples are oriented, although to a somewhat lesser degree than for $YBa_2Cu_3O_7$. The alignment of its *c* axis normal to $YBa_2Cu_3O_7$ E||H is evident. The induced magnetization in SCO is therefore orthogonal to the *c* axis, unlike all other cuprates where the *c* axis orients strongly along the field direction. SCO maintains at least some of the magnetic anisotropy from the CuO_2 chains in undoped Sr_2CuO_3 (40) despite its tetragonal space group. This confirms the prior suggestion that the crystal structure is incomplete, augmented by showing that the properties of SCO are coupled to these extracrystallographic factors. The unique direction parallel to the magnetization will be labeled "*a*," the orthogonal direction in the Cu planes "*b*."

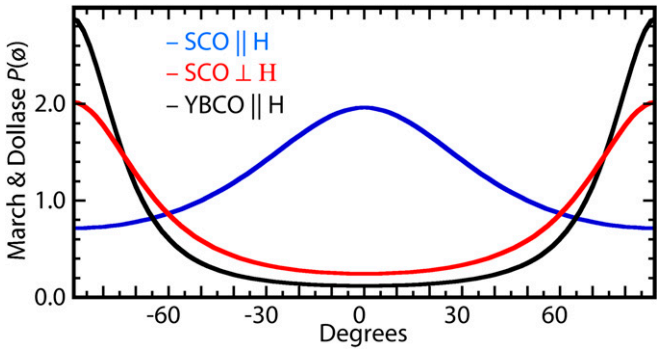

Fig. 1. March and Dollase probability factors (39) for sample orientation in magnetic field. The result for the $YBa_2Cu_3O_7$||H sample that was prepared in the same mold as the SCO||H sample is included for reference to show the 90° rotation of the (001) axis (*c* axis) of the two compounds.

The capabilities and limitations of EXAFS in elucidating structure and dynamics in correlated materials are described in *SI Appendix*. The original EXAFS spectrum, $\chi(\mathbf{k})$, is best presented as its Fourier transform, $\chi(R)$, because the modulus peaks that originate in the constituent waves of the original $\chi(\mathbf{k})$ correspond to the contributions of the neighbor atom shells arranged from short to long absorber–neighbor distances to give an approximate representation of the partial pair distribution. Inspection of the Fourier transforms of the Cu K EXAFS of the two orientations (Fig. 2) show the same Sr and Cu contributions at, respectively, $R = 2.9$ and 3.5 Å. The contribution of the Cu neighbors in both the *a* and *bc*-oriented spectra differs from all other cuprates where it occurs only in E||*ab* spectra, corroborating this unique orientation found in the diffraction. Curve-fitting analysis finds 3.79 Å Cu-Cu distances. An identical Cu-Cu distance for both orientations demonstrates that the tetragonal symmetry found crystallographically is intrinsic and not the result of small, orthorhombic domains averaging to tetragonal. The amplitudes of the Cu signals that are ∼40% of the amount displayed by other cuprates (29, 41) are also consistent with a division of the Cu contribution between the two orientations. The Cu-Sr pair is best fit with the principal and a smaller shell separated by an amount just above the resolution limit, 3.22/3.35-Å Cu-Sr distances for E||H and 3.24/3.38 Å for E⊥H. These are equal within the uncertainty for the two orientations. This result is indicative of an overall anharmonic distribution. The Cu-Cu and principal Cu-Sr distances are within 0.01–0.02 Å of the crystallographic values.

If the O sublattice is tetragonal then all of the Cu-O distances in the E||H spectrum from the *aa* plane must be found in the E⊥H spectrum, with any additional ones belonging to the *c* component. Deviation of the O positions from the tetragonal symmetry of the Cu-Sr sublattice is evident in the comparison of the locations of the peaks of the two spectra (Fig. 2). Unlike the tetragonal arrangement of the Cu and Sr atoms, the O sublattice is therefore orthorhombic with distinct *a* and *b* axes but insufficiently ordered to give a clear signature in the diffraction pattern dominated by the Cu and Sr. The E||H spectrum measures the *a* components of the Cu pair distribution. The O region of the spectrum for E||H is dominated by a single peak (Fig. 2*A*) (29, 42). Complete curve fits, however, require three O neighbors at 1.92, 2.09, and 2.31 Å, with a fourth low-amplitude shell at 2.64 Å giving a small improvement in the fit (Fig. 2 *A*, *Inset* and *SI Appendix*, Fig. S3). The 1.92-Å Cu-O distance is close to half of the 3.79-Å Cu-Cu distance. The E⊥H spectrum displays three distinct peaks in the O neighbor region. The lower position of the first one demonstrates a shorter Cu-O distance than in the *a* direction, just as the other peaks at higher R signify longer ones. This complicated spectrum is fit by four O neighbors at 1.83, 2.00, 2.27, and 2.61 Å (Fig. 2 *B*, *Inset*). An additional small feature in both spectra at R ∼ 2.5 Å is fit by Sr and/or O at ∼2.8–2.9 Å. The 1.83- and 2.00-Å distances with their equivalent amplitudes could be the two parts of an off-center O in a *b*-oriented -Cu-O- chain and/or two Cu-Oap distances of a

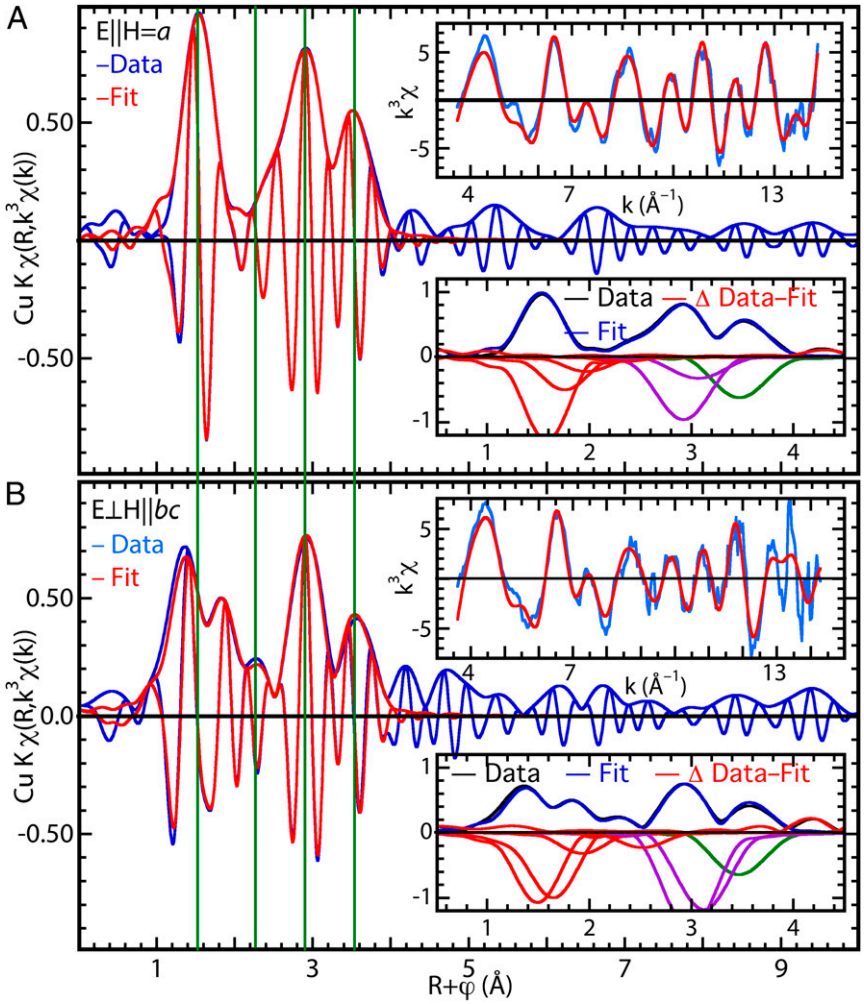

Fig. 2. EXAFS [Fourier transform or χ(R) representation] of SCO (*A*) along the same direction as the magnetic field and (*B*) perpendicular to the magnetic field. The main figures show the data and fit in real space, the *Upper Right Insets* the data and fits in the original (before Fourier transformation) momentum (k)/energy domain, and the *Lower Right Insets* show the Fourier transform moduli of the data, fits, and differences in their upper halves and the contributions of the individual neighbor shells, inverted for clarity, in their lower halves. The vertical green lines trace the position of the spectral features for, from low to high, the O neighbor at 1.92 Å, the O neighbor at 2.6 Å, the Sr neighbors, and the Cu neighbors with a bridging O ion between them. The relative numbers of atoms are reflected by the peak amplitudes, reduced by $1/R^2$.

distorted square Cu site with O vacancies in the *ab* plane. The differences between 1.83, 1.92, 2.00, and 2.09 Å are significantly larger than the normal EXAFS error ±0.02 Å, confirming the separate *a* and *b* Cu-O distributions and division of the spectra into *a* and the combined *bc* component. Since the Cu-Cu wave in $\chi(\mathbf{k})$ in both spectra is defined by the amplitudes and phases of the Cu-O-Cu moiety with the bridging O, a corresponding fraction of the 1.83- and 2.00-Å Cu-O pairs in the *bc*-oriented spectrum must be the bridging O of the Cu-O-Cu pairs along the *b* axis. Remaining O neighbors may be Oap, including the O at the longer distances if Sr displacements allow expansion of the Cu–Oap bond.

Insofar as the most significant finding of this study is the location of the O ions and vacancies in the *aa*-oriented Cu planes a thorough analysis was performed that provides a graphic presentation of the relevant results. As explained previously, the 0.11-Å resolution derived from the upper limit of the spectra ensures that the individual Cu-O waves in $\chi(\mathbf{k})$ in the E||*a* spectrum are easily separable. Rather than rely solely on curve-fit results, the location of the O vacancies is addressed by directly comparing the isolated Cu-O-Cu and Cu-O EXAFS waves against appropriate standards, in this case the same waves from, respectively, the E||*bc*-oriented spectra and the E||*a* spectra from $YBa_2Cu_{2.75}Mo_{0.25}O_{7.54}$ that we have shown has fully ordered CuO_2 planes and CuO_3-type chains. This comparison not only gives the relative numbers of Cu-O-Cu pairs and bridging O in the E||H||*a* spectrum by direct comparison of their magnitudes but also tests the extent to which their originating structures are identical via the similarity of their phases and amplitude envelopes. The Cu-O-Cu waves in $\chi(\mathbf{k})$ from the two orientations (Fig. 3*A*) are almost identical, verifying this assignment and the presumption that uncorrelated thermal motion makes the contributions of any unbridged Cu-Cu pairs negligible. Deriving the relative numbers of Cu atoms requires correcting the spectral amplitudes by the polarization geometry factors of 3 for the E||H||*a* spectrum and 3/2 for the E⊥H||*bc* (43). The essentially identical amplitudes therefore demonstrate that the numbers of Cu-O-Cu neighbors and therefore bridging O in the *a* direction are only close to half that for *b*. The *a*-oriented, partial -Cu-O- chains and presumably the mixed Cu(II, III) valence resulting from the added charge from the excess O account for the conversion of the rectangular arrangement of the Cu and Sr atoms of Sr_2CuO_3 to their square geometry in SCO, even while the O atoms separate into different arrangements along the *a* and *b* directions so that their sublattice has orthorhombic

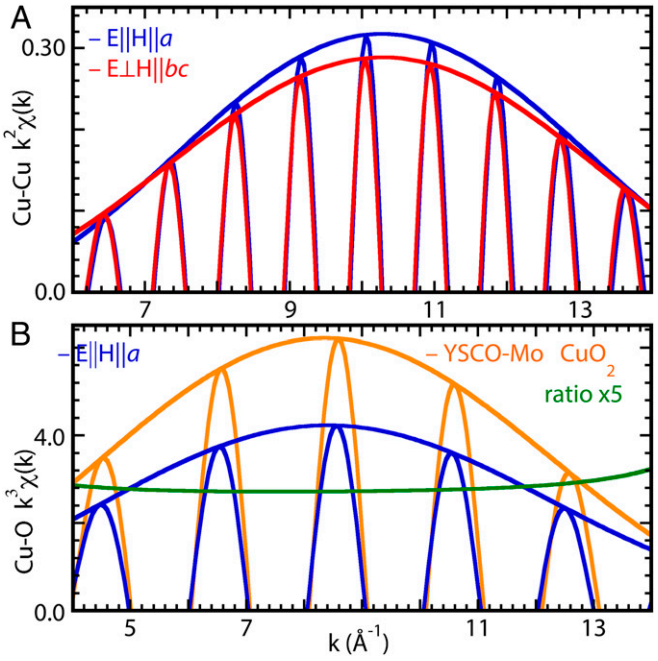

Fig. 3. EXAFS waves and amplitudes for direct comparison of relative atom numbers. (*A*) The Cu-Cu EXAFS from the two orientations of SCO. (*B*) The nearest-neighbor Cu-O waves and amplitudes from the *a* orientation of SCO and the *ab* orientation of $YSr_2Cu_{2.75}Mo_{0.25}O_{7.54}$ and the ratio of the amplitudes ×5. The Cu-O-Cu and Cu-O EXAFS from the spectra were separated by subtracting all of the other components (Fig. 2) from the fits followed by Fourier back-transformation over the width of the spectral feature from the Cu. These are the original waves; converting to relative numbers of atoms from the amplitude ratios requires the polarization correction described in the text.

symmetry (40). This same parameter is obtained independently by comparing the Cu-O wave from the E||H||*a* spectrum with the one from $YSr_2Cu_{2.75}Mo_{0.25}O_{7.54}$ (Fig. 3*B*) with its known structure (6). The amplitude ratio is 0.6–0.7. After the same factor of 2 polarization correction, the corrected amplitude of 0.35 times the average 3–1/3 O/Cu neighbors in $YSr_2Cu_{2.75}Mo_{0.25}O_{7.54}$ gives ~1.1 O atoms in the *a* direction for SCO. The numbers of O and Cu neighbors therefore show that the *b*⊥H -Cu-O- chains are essentially intact from Sr_2CuO_3 and the *a*||H -Cu-O- chains are around half filled (Fig. 4*A*). This half filling corresponds to the Cu(II):(III) ratio.

Since ordering of the O vacancies in the *b*-oriented -Cu-O- chains would be observed in the diffraction, these are likely located aperiodically. However, within the constraints of an aperiodic distribution it is still possible that the O atoms in these -Cu-O- chains cluster. At one extreme there is no cooperativity between them, these O atoms are located randomly, and their overall distribution is homogeneous on a scale sufficiently large to overcome small deviations (Fig. 4*A*). This random distribution results in Cu ions with two, three, and four O neighbors within the *aa* Cu plane whose Cu-O distances would be close to half of the 3.79-Å distance between the pairs of Cu atoms that they bridge as in La_2CuO_4 (Fig. 4*D*). At the other extreme these O atoms may cluster into domains with the ordered CuO_2 plane structure (Fig. 4 *C* and *E*) whose only restriction is that their size must be below the diffraction limit, which becomes larger if these domains are aperiodically distributed in the material. This distribution results in a heterogeneous, nanophase separated structure. Intermediate distributions that would be inhomogeneous (Fig. 4*B*) are not antithetical to any of these considerations. However, which of these possibilities actually occurs does have consequences. If these O atoms are fully clustered then it is easily understood that the superconductivity resides in the CuO_2 domains, enabled by the short pair-correlation lengths, and would be very similar to conventional cuprates except it would percolate between the domains instead of flowing unobstructed. In contrast, in the homogeneous distribution, the superconductivity would be quenched at either the vacancy or occupied sites and therefore filamentary. For $YSr_2Cu_{2.75}Mo_{0.25}O_{7.54}$, the Mo served as a probe for its own organization (6), but there is no comparable probe for the O atoms within SCO. However, our unpublished EXAFS spectra over a range of temperatures are more consistent with the random, homogeneous type of structure.

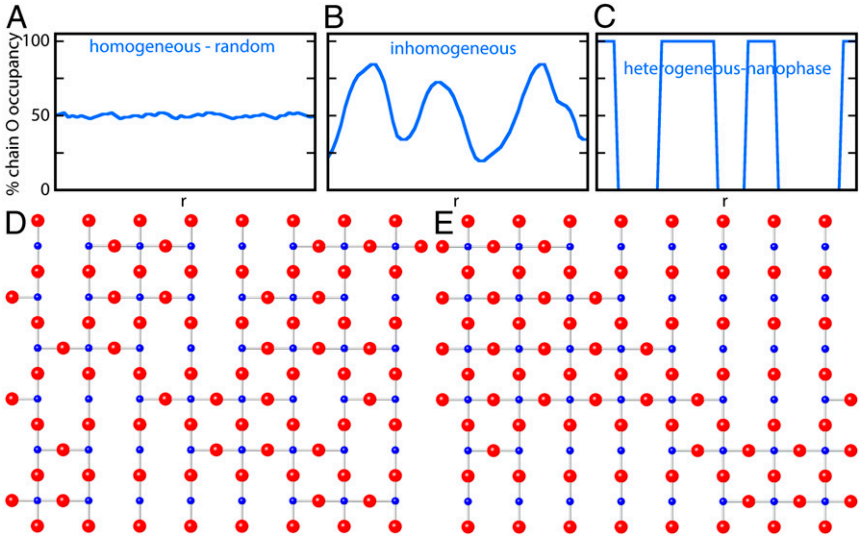

Fig. 4. Conceptual depictions of O vacancies in $Sr_2CuO_{3.3}$. The *a*-oriented -Cu-O- chain occupancy distribution (occupancy vs. r, where r is defined as location on a trajectory through the Cu plane) for: (*A*) a random, homogeneous distribution caused by no cooperation between the O atoms; (*B*) a moderate tendency for clustering resulting in an inhomogeneous distribution; (*C*) a strong tendency for clustering causing nanophase separation and a heterogeneous structure composed of domains below the diffraction limit in size consisting of either CuO_2 planes or -Cu-O- chains. (*D*) The corresponding structure of *A*. (*E*) The corresponding structure of *C*.

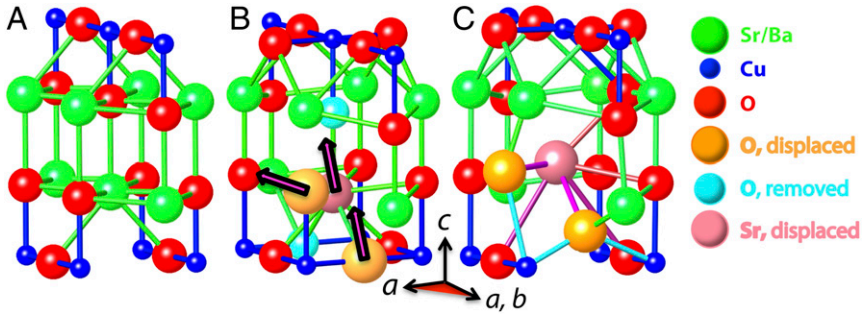

Fig. 5. Conceptual depictions of possible displacements in $Sr_2CuO_{3.3}$. (*A*) Sr_2CuO_3 with the Cu-O chains at the bottom, (*B*) the T structure of La_2CuO_4 with the CuO_2 planes derived from the Cu-O chains by the insertion of O bridges between the Cu pairs on the *b* axis of Sr_2CuO_3 at the bottom, and (*C*) $Sr_2CuO_{3.3}$ with the Cu atoms in the *ab* planes at the bottom and Oap and one of the bridging O atoms removed. The structure in *C* with Sr is produced from *B* with La by removing the central apical and a *b*-oriented Cu-O- chain O atoms and displacing the central Sr atom and two of its O neighbors in the directions of the arrows in *B*, with expanded Sr–O bonds magenta and pink, expanded Cu–O bonds turquoise. The Oap vacancy in SCO creates a large volume for the Sr atom that the chain O vacancy renders asymmetric. The O excess results in comparable amounts of Cu(II) and (III). The displacement of the Sr atom accompanied by a rotation of the O-Cu-O moiety around the *b* axis is a possible mechanism for giving the longer Cu-O distances found by the EXAFS. These motions would be facilitated by cooperative action of the atoms in neighboring unit cell in which the inverse motions are synchronized so that this extended set of atoms oscillate between this structure and its mirror image coherently as a tunneling polaron.

The remaining issue for the structure is local, the disposition of the O neighbors with Cu-O distances greater than 2 Å and the possibility of Sr at ∼2.8 Å. Assigning formal charges or valence, the Cu with four O neighbors therefore already has the preferred Cu^{2+} square planar geometry if Oap are missing or at longer distances that may be tilted from the *c* axis. Similarly, if the Oap are at their Sr_2CuO_3 positions then the Cu ions with two *a*-chain O vacancies will have the same Cu(II) assignment with the axial positions on the *a* chain vacant. This scenario implies that the Cu ions with three O neighbors from the plane would be Cu(III), which accommodates a wider range of geometries that would include their Oap neighbors. Consistent with the added charge, each adventitious O therefore results in ∼2 Cu(III) and a similar number of O in *a*-oriented -Cu-O- chains, with the second O coming from a displacement of an Oap into the bridging position in the chain. The varying Cu geometries will give the range of Cu-Oap distances, with disorder reducing the EXAFS amplitudes. Further insight is gained by tracking the evolution of the structure from Sr_2CuO_3 to T-La_2CuO_4 at the Sr site. The Sr in Sr_2CuO_3 has seven O nearest neighbors with Sr-O distances in a narrow range around 2.5 Å (Fig. 5*A*), whereas La_2CuO_4 has eight La-O from 2.6 to 2.8 Å and a ninth very short one to the apical O at 2.36 Å (Fig. 5*B*). Sr_2CuO_3 is presumably stable because of its high local symmetry and uniform Cu(II). In SCO this symmetry is destroyed by the half-filled *b*-oriented Cu-O- chains, apical O vacancies, and the mixed Cu valence. The noninteger bulk stoichiometry will also result in unit cells with different compositions and structures whose distribution lacks translational symmetry. The removal of the apical O opens an extremely large space for the Sr (Fig. 5*C*). Displacements of the Sr in combination with the Cu(II, III) mixture would cause collective displacements and highly unusual Sr and Cu geometries. One such possibility, a rotation of a CuO_2 moiety, is depicted (Fig. 5*C*). The longer Cu-O pairs could thus be Cu-Oap expanded because of the displaced Sr. The very short ∼2.8-Å Cu-Sr distance that gives the best fits of the Cu EXAFS at some temperatures would thus be somewhat analogous to the 2.7-Å Cu-Cu distances in the alkali metal $MCuO_2$ compounds, here caused by bent, double-O bridges.

The question of the whether the O vacancies are located in the apical positions or in highly disrupted CuO_2 planes is therefore moot; they are located in both positions. The vacancies will result in substantial displacements of the O ions to give Cu and Sr geometries compatible with the Cu(II, III) combination. Collective and cooperative effects could be expected to result in preferred configurations of sets of atoms, but these would be positioned aperiodically throughout the crystal. Solving the structure in the tetragonal space group would give the average position of their projections onto the axes through the nearest Cu. In contrast, EXAFS gives a more complete depiction of this system because of its sensitivity to local order. The unpaired electron density along the *a*-oriented Cu-O chains resides in a different orbital than in other cuprates, and the *a*-*b* anisotropy rotates the magnetization. Superconductivity in the disrupted $CuO_{1.5}$ planes has been described: either percolation of the short coherence length superconductivity that resides in domains with the conventional CuO_2 structure, or filamentary superconductivity through continuous Cu-O networks. If ordered, two-dimensional structures with Cu and O atoms are required there is an alternative: planes in the *c* direction with Sr that still have a square sublattice of Cu but with a type of Cu-Sr-O unit that will have different Cu energy levels and occupations. These unique attributes of the composition, structure, magnetism, and other properties of SCO demonstrate the existence of a class of exotic superconductors. This class of materials would have the second-highest transition temperature after conventional cuprates. Under certain conditions, superconductivity can occur just as effectively via more structurally complex alternatives to the ubiquitous CuO_2 planes.

Materials and Methods

Single-phase SCO with T_c = 95 K (*SI Appendix*, Fig. S1) and 19% superconducting volume fraction was prepared by annealing Sr_2CuO_3 and $KClO_4$ in amounts giving a nominal composition of $Sr_2CuO_{3.3}$ at around 7 GPa and 1,050 °C for 30 min (17, 18). The XAFS samples were prepared by having a mixture of the $Sr_2CuO_{3.3}$ in epoxy set in the bore of a 16-T magnet. X-ray diffraction analysis of these samples showed only the $Sr_2CuO_{3.3}$ pattern (*SI Appendix*, Fig. S2). XAFS was measured in the continuous transmission mode on beamline 2–2 at the Stanford Synchrotron Radiation Lightsource. XAFS spectra were analyzed by standard methods (44) with curve fits using amplitudes and phases calculated by the feff9 code (45). A more detailed description is found in *SI Appendix*. Original data are available from S.D.C. on request (st3v3n.c0nrads0n@icloud.com).

ACKNOWLEDGMENTS. The authors acknowledge the financial support from the Slovenian Research Agency (Research Core Funding P1-0040). Work at Washington State University is partially supported by the US National Science Foundation (NSF) Division of Materials Research Early Concept Grants for Exploratory Research Grant 1928874. Work at Institute of Physics, Chinese Academy of Sciences (IOPCAS) was supported by Ministry of Science and Technology (MOST) and National Natural Science Foundation (NSF) of China of China through Research Projects 2018YFA03057001, 2017YFA0302901, 11820101003, 2016YFA0300301, 2015CB921000, and 112111KYS820150017. Use of the Stanford Synchrotron Radiation Lightsource, SLAC National Accelerator

Laboratory, is supported by the US Department of Energy, Office of Science, Office of Basic Energy Sciences under Contract DE-AC02-76SF00515. Work at Stanford and SLAC is supported by the Stanford Institute for Materials and Energy Science, SLAC National Accelerator Laboratory, under Department of Energy, Office of Basic Energy Sciences Contract DEAC02-76SF00515.

1. J. G. Bednorz, K. A. Muller, Possible high-tc superconductivity in the Ba-La-Cu-O system. *Z. Phys. B Condens. Matter* **64**, 189–193 (1986).
2. B. Keimer, S. A. Kivelson, M. R. Norman, S. Uchida, J. Zaanen, From quantum matter to high-temperature superconductivity in copper oxides. *Nature* **518**, 179–186 (2015).
3. A. Ono, Superconductivity in Cr-1212 cuprates $Sr_{2-x}Ba_xYCu_{2.8}Cr_{0.2}O_z$. *Jpn. J. Appl. Phys. Pt. 2* **34**, 1528–1531 (1995).
4. A. Ono, Oxygenation and critical-temperature optimization in M-1212 cuprates (Sr, Ba)(2)YCu(2.8)M(0.2)O(z) (M=Ti, Ga, Ge, Al). *Jpn. J. Appl. Phys.* **35**, L201–L204 (1996).
5. D. Haskel, E. A. Stern, D. G. Hinks, A. W. Mitchell, J. D. Jorgensen, Altered Sr environment in $La_{2-x}Sr_xCuO_4$. *Phys. Rev. B* **56**, R521–R524 (1997).
6. S. D. Conradson *et al*., Local lattice distortions and dynamics in extremely overdoped superconducting $YSr_2Cu_{2.75}Mo_{0.25}O_{7.54}$. *Proc. Natl. Acad. Sci. U.S.A.* **117**, 4559–4564.
7. A. Gauzzi *et al*., Bulk superconductivity at 84 K in the strongly overdoped regime of cuprates. *Phys. Rev. B* **94**, 180509 (2016).
8. W. M. Li *et al*., Superconductivity in a unique type of copper oxide. *Proc. Natl. Acad. Sci. U.S.A.* **116**, 12156–12160 (2019).
9. D. Rybicki, M. Jurkutat, S. Reichardt, C. Kapusta, J. Haase, Perspective on the phase diagram of cuprate high-temperature superconductors. *Nat. Commun.* **7**, 11413 (2016).
10. E. S. Bozin *et al*., Charge-screening role of c-axis atomic displacements in $YBa_2Cu_3O_{6+x}$ and related superconductors. *Phys. Rev. B* **93**, 054523 (2016).
11. Y. Y. Peng *et al*., Influence of apical oxygen on the extent of in-plane exchange interaction in cuprate superconductors. *Nat. Phys.* **13**, 1201–1206 (2017).
12. S. Kim, X. Chen, W. Fitzhugh, X. Li, Apical charge flux-modulated in-plane transport properties of cuprate superconductors. *Phys. Rev. Lett.* **121**, 157001 (2018).
13. M. Takano, M. Azuma, Z. Hiroi, Y. Bando, Y. Takeda, Superconductivity in the Ba-Sr-Cu-O system. *Physica C* **176**, 441–444 (1991).
14. W. M. Li *et al*., Synthesis and structure stability of $Ba_2CuO_{3+delta}$ under high pressure. *Int. J. Mod. Phys. B* **29**, 15420242 (2015).
15. Z. Hiroi, M. Takano, M. Azuma, Y. Takeda, A new family of copper-oxide superconductors $Sr_{N+1}Cu_NO_{2N+1+delta}$ stabilized at high-pressure. *Nature* **364**, 315–317 (1993).
16. H. Yang, Q. Q. Liu, F. Y. Li, C. Q. Jin, R. C. Yu, TEM and EELS characterization of a $Sr_2CuO_{3+delta}$ superconductor post-annealed at different temperatures: Enhancement of T-c by apical oxygen reordering. *Supercond. Sci. Technol.* **20**, 904–910 (2007).
17. W. Liang *et al*., Growth of $Sr_2CuO_{3+delta}$ superconductor single crystals at high pressure. *Sci. China Phys. Mech. Astron.* **56**, 691–693 (2013).
18. Y. Liu *et al*., A new modulated structure in $Sr_2CuO_{3+delta}$ superconductor synthesized under high pressure. *Physica C* **497**, 34–37 (2014).
19. P. S. Hafliger *et al*., Quantum and thermal ionic motion, oxygen isotope effect, and superexchange distribution in La_2CuO_4. *Phys. Rev. B* **89**, 085113 (2014).
20. C. L. Teske, H. Muller-Buchsbaum, Alkaline earth metals oxocuprate. 2. Sr_2CuO_3. *Z. Anorg. Allg. Chem.* **371**, 325 (1969).
21. K. R. Thurber, A. W. Hunt, T. Imai, F. C. Chou, 17O NMR study of q = 0 spin excitations in a nearly ideal S = 1 / 2 1D Heisenberg antiferromagnet, Sr2CuO3, up to 800 K. *Phys. Rev. Lett.* **87**, 247202 (2001).
22. P. Laffez, X. J. Wu, S. Adachi, H. Yamauchi, N. Môri, Synthesis of superconducting $Sr_2CuO_{3+delta}$ using high-pressure techniques. *Physica C* **222**, 303–309 (1994).
23. T. H. Geballe, M. Marezio, Enhanced superconductivity in Sr_2CuO_{4-v}. *Physica C* **469**, 680–684 (2009).
24. T. Egami *et al*., Local structural anomaly near T_c observed by pulsed neutron-scattering. *Physica C* **185–189**, 867–868 (1991).
25. M. I. Salkola, A. R. Bishop, J. Mustre de Leon, S. A. Trugman, Dynamic polaron tunneling in $YBa_2Cu_3O_7$: Optical response and inelastic neutron scattering. *Phys. Rev. B Condens. Matter* **49**, 3671–3674 (1994).
26. M. I. Salkola, A. R. Bishop, S. A. Trugman, J. Mustre de Leon, Correlation-function analysis of nonlinear and nonadiabatic systems: Polaron tunneling. *Phys. Rev. B Condens. Matter* **51**, 8878–8891 (1995).
27. J. M. DeLeon *et al*., "X-ray absorption fine structure applied to the study of systems with lattice instabilities" in *Applications of Synchrotron Radiation Techniques to Materials Science III*, L. J. Terminello, S. M. Mini, H. Ade, D. L. Perry, Eds. (Materials Research Society Symposium Proceedings, Cambridge University Press, 1996), vol. 437, pp. 189–199.
28. A. R. Bishop, D. Mihailovic, J. M. de Leon, Signatures of mesoscopic Jahn-Teller polaron inhomogeneities in high-temperature superconductors. *J. Phys. Condens. Matter* **15**, L169–L175 (2003).
29. S. D. Conradson, I. D. Raistrick, A. R. Bishop, Axial oxygen-centered lattice instabilities and high-temperature superconductivity. *Science* **248**, 1394–1398 (1990).
30. C. A. Young *et al*., Reverse Monte Carlo study of apical Cu-O bond distortions in $YBa_2Cu_3O_{6.93}$. *Z. Kristallogr. Cryst. Mater.* **227**, 280 (2012).
31. M. Arai *et al*., Local structural instability of high-T_c oxide superconductors studied by inelastic neutron-scattering. *J. Supercond.* **7**, 415–418 (1994).
32. S. D. Conradson, I. Batistic, A. R. Bishop, J. Mustre de Leon, Evidence for an axial oxygen-centered lattice fluctuation associated with the superconducting transition in $YBa_2Cu_3O_7$. *Phys. Rev. Lett.* **65**, 1675–1678 (1990).
33. I. Batistic, A. R. Bishop, S. D. Conradson, S. A. Trugman, J. Mustre de Leon, Polaron origin for anharmonicity of the axial oxygen in $YBa_2Cu_3O_7$. *Phys. Rev. Lett.* **68**, 3236–3239 (1992).
34. P. G. Allen, S. D. Conradson, A. R. Bishop, A. R. Bishop, J. Mustre de Leon, Characterization of a split axial-oxygen site in $TlBa_2Ca_3Cu_4O_{11}$ by extended x-ray-absorption fine-structure spectroscopy. *Phys. Rev. B Condens. Matter* **44**, 9480–9485 (1991).
35. J. M. Deleon *et al*., Planar oxygen-centered lattice instabilities in Tl-based high-temperature superconductors. *Physica C* **220**, 377–382 (1994).
36. S. D. Conradson *et al*., Possible demonstration of a polaronic Bose-Einstein(-Mott) condensate in $UO_{2(+x)}$ by ultrafast THz spectroscopy and microwave dissipation. *Sci. Rep.* **5**, 15278 (2015).
37. S. D. Conradson *et al*., Closure of the Mott gap and formation of a superthermal metal in the Frohlich-type nonequilibrium polaron Bose-Einstein condensate in UO_{2+x}. *Phys. Rev. B* **96**, 125114 (2017).
38. G. Fabbris, M. Hücker, G. D. Gu, J. M. Tranquada, D. Haskel, Combined single crystal polarized XAFS and XRD at high pressure: Probing the interplay between lattice distortions and electronic order at multiple length scales in high T-c cuprates. *High Press. Res.* **36**, 348–359 (2016).
39. W. A. Dollase, Correction of intensities for preferred orientation in powder diffractometry–Application of the march model. *J. Appl. Cryst.* **19**, 267–272 (1986).
40. J. Schlappa *et al*., Probing multi-spinon excitations outside of the two-spinon continuum in the antiferromagnetic spin chain cuprate Sr_2CuO_3. *Nat. Commun.* **9**, 5394 (2018).
41. S. D. Conradson, I. Batistic, A. R. Bishop, A. R. Bishop, J. Mustre de Leon, Correlation between axial-oxygen anharmonicity and T_c in $YBa_2Cu_3O_7$ and related compounds. *Phys. Rev. B Condens. Matter* **44**, 2422–2425 (1991).
42. S. D. Conradson *et al*., Axial oxygen-centered lattice instabilities in $YBa_2Cu_3O_7$: An application of the analysis of extended x-ray-absorption fine structure in anharmonic systems. *Phys. Rev. B Condens. Matter* **45**, 2447–2457 (1992).
43. A. Manceau, D. Chateigner, W. P. Gates, Polarized EXAFS, distance-valence least-squares modeling (DVLS), and quantitative texture analysis approaches to the structural refinement of Garfield nontronite. *Phys. Chem. Miner.* **25**, 347–365 (1998).
44. S. D. Conradson *et al*., Nanoscale heterogeneity, premartensitic nucleation, and a new plutonium structure in metastable delta fcc Pu-Ga alloys. *Phys. Rev. B Condens. Matter Mater. Phys.* **89**, 224102 (2014).
45. J. J. Rehr, J. J. Kas, F. D. Vila, M. P. Prange, K. Jorissen, Parameter-free calculations of X-ray spectra with FEFF9. *Phys. Chem. Chem. Phys.* **12**, 5503–5513 (2010).